Acta Mechanica 176, 231–243 (2005)
DOI 10.1007/s00707-004-0206-y

Acta Mechanica
Printed in Austria

Buckling analysis of a plate with built-in rectangular delamination by strip distributed transfer function method

D. Li, G. Tang, J. Zhou, and **Y. Lei**, Changsha, China

Received April 30, 2003; revised October 11, 2004
Published online: March 7, 2005

Summary. Delamination may reduce the buckling of the laminated plate. In this paper, a semi-analytical, semi-exact method, namely the strip transfer function method based on Mindlin's first-order shear deformation theory is developed to investigate the buckling of a delaminated plate. First, a composite plate with bulit-in rectangular delamination is divided into two kinds of rectangular super-units, one with a delamination and one without. The variational principle is used to obtain equilibrium equations and boundary conditions. Then, by displacement continuity and force balance of nodes that connect two super-units, the characteristic equation for the buckling analysis of the delaminated plate is derived. Consequently, buckling load and mode are computed. By comparing the results of the plate with through-the–width delamination to the analytic solutions of a beam and the results of the finite element method, the validity of this method is tested. Furthermore, the influence of length, depth and position of the delamination, the boundary condition and the plying angle of the material on the buckling load is analyzed.

1 Introduction

Delaminations of different shapes might emerge in fiber-reinforced composite structures during their manufacturing and using process. Delamination has great influence on the loading capacity of structures under axial compression load especially when a local buckling mode exists, which cannot be ignored. Thus it is of much theoretical and practical significance to research the influence of delamination on the loading capacity of structures and to analyze different types of buckling modes for delaminated structures.

Many researchers have been studying the local buckling and post-buckling characteristics of structures with surface delaminations using the Rayleigh-Ritz method in recent years. Considering the effects of stretching-shearing coupling and bending-twisting coupling, Chen and Li [1], [2] performed the theoretical and experimental studies on the buckling characteristics of composite laminates with rectangular, elliptic or belt-shape surface delaminations. Yin and Jane [3], [4] gained the buckling and post-buckling solutions for laminates with elliptic anisotropic delaminations and pointed out the lowest order in the Rayleigh-Ritz method to get force, moment and energy releasing rate as results with adequate precision. Zhang and Yu [5] analyzed the axial symmetric and non-symmetric buckling problems for laminates with circular delaminations in further detail.

Instead of applying analytic or semi-analytic methods, the structures with various shapes of built-in delaminations were analyzed using the finite element method (FEM) [6], [7]. Although

the FEM is the most powerful and versatile tool for different structural systems including delaminated plates, it does have some drawbacks as a numerical method. Actually, it is computationally intensive, needs large amounts of computer memory and does not provide explicit and closed-form solutions.

In this paper, a semi-analytical, semi-exact method, namely the strip transfer function method based on Mindlin's first-order shear deformation theory is used to analyze the buckling problems of a laminated plate with a bulit-in rectangular delamination. The delaminated plate is divided into two kinds of rectangular super-units. In lateral direction, those super-units are dispersed into many strip elements. Unlike in the FEM, the displacement field of the super-units is interpolated by polynomials in terms of nodal line displacements, which are functions of the strip longitudinal coordinate. The strip distributed transfer function method is used to get the exact and closed-form solution of the super-unit along the strip longitudinal direction. Finally, the buckling load and mode of the delaminated plate are computed with higher accuracy and efficiency through a special treatment for the super-units with a delamination and a synthesized method. However, it should be noticed that the possible contact between delamination surfaces in particular cases is not taken into consideration at present.

2 Super-unit model

For studying the buckling problem of a delaminated plate, two types of super-units are considered. One (Fig. 1a) is a general super-unit without delamination, and the other (Fig. 1b) is a delaminated super-unit including a delamination. The general super-unit is dispersed into NS rectangular strip elements by $(NS+1)$ nodal lines in lateral direction. The j-th strip element of width b_j includes the j-th and the $(j+1)$-th nodal line and four nodes (Fig. 2). Oxy is the local coordinate system for the j-th strip element and o lies at the center of the j-th nodal line. As for the delaminated super-unit, the dispersing method is varied. Because of delamination in $A_1B_1C_1D_1$, the delaminated region is split into two sublaminates as top and bottom. So there are three nodal lines at a delamination tip A_1B_1 or C_1D_1: two nodal lines belonging to the top and bottom sublaminate, respectively, in the delaminated region, and another nodal line in the undelaminated region. And there are two nodal lines in the top and bottom sublaminates at E_1F_1 in the delaminated region, respectively.

The j-th nodal line displacements are written as

$$u_j(x,z) = u_{0j}(x) + z\psi_{xj}(x), \tag{1.1}$$

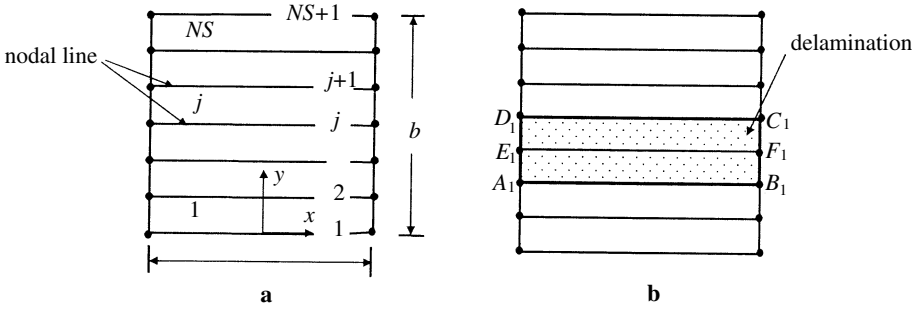

Fig. 1. Rectangular super-elements

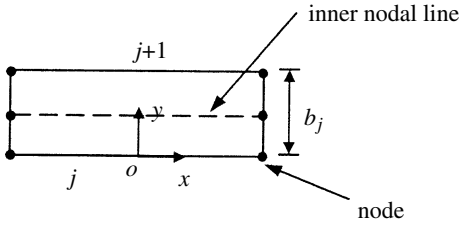

Fig. 2. The j-th strip element

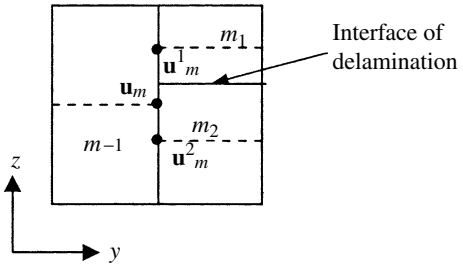

Fig. 3. Relation among displacements of nodal lines at the delamination tip (a point denotes a nodal line)

$$v_j(x,z) = v_{0j}(x) + z\psi_{yj}(x), \tag{1.2}$$

$$w_j(x,z) = w_{0j}(x), \tag{1.3}$$

in which $u_{0j}(x)$, $v_{0j}(x)$' $w_{0j}(x) \sim$ and $\psi_{xj}(x)$, $\psi_{yj}(x)$ are the j-th nodal line shifting and rotational displacement components, respectively.

The vector composed of all of the above-defined displacement functions of the j-th nodal line can be written as

$$\mathbf{u}_j(x) = \{u_{0j}(x)\ \psi_{xj}(x)\ v_{0j}(x)\ \psi_{yj}(x)\ w_{0j}(x)\}^T, \tag{2}$$

where the superscript T denotes the transpose of the matrix.

In order to increase the interpolation precision, the inner nodal line and the corresponding displacement vector $\boldsymbol{\lambda}_j(x)$, whose definition is similar to $\mathbf{u}_j(x)$, are introduced for each strip element. By doing this we can increase the calculating precision without influence on the harmonization between two elements. Therefore, the nodal line displacement vector of the j-th strip element is defined as

$$\mathbf{W}_j(x) = \{\mathbf{u}_j^T(x)\ \boldsymbol{\lambda}_j^T(x)\ \mathbf{u}_{j+1}^T(x)\}^T. \tag{3}$$

For the strip element $m_k(k = 1,2)$ at a delamination tip (A_1B_1 or C_1D_1 in Fig. 1b), the displacement vector $\mathbf{u}_m^k(x)$ at the tip is related to the nodal line displacement vector $\mathbf{u}_m(x)$ in the no-delamination strip element $m-1$ (Fig. 3). Their relationship is

$$\mathbf{u}_m^k(x) = \mathbf{T}_{mk}\mathbf{u}_m(x), \tag{4}$$

where

$$\mathbf{T}_{mk} = \begin{bmatrix} \mathbf{G}_k & \mathbf{0}_{2\times2} & \mathbf{0}_{2\times1} \\ \mathbf{0}_{2\times2} & \mathbf{G}_k & \mathbf{0}_{2\times1} \\ \mathbf{0}_{1\times2} & \mathbf{0}_{1\times2} & 1 \end{bmatrix}, \quad \mathbf{G}_k = \begin{bmatrix} 1 & d_k \\ 0 & 1 \end{bmatrix},$$

and $\mathbf{0}_{i\times j}$ is an $i \times j$ zero matrix and d_k is the relative location in z-direction between the middle surface of the strip element m_k and $m-1$.

Let the strip element m_k be the k-th strip element. Consequently, the nodal line displacement vector is expressed as

$$\mathbf{W}_k(x) = \bar{\mathbf{T}}_{mk}\{\mathbf{u}_m^T(x)\ \boldsymbol{\lambda}_k^T(x)\ \mathbf{u}_{k+1}^T(x)\}^T, \tag{5}$$

in which $\bar{\mathbf{T}}_{mk} = \begin{bmatrix} \mathbf{T}_{mk} & \mathbf{0}_{5\times 10} \\ \mathbf{0}_{10\times 5} & \mathbf{I}_{10} \end{bmatrix}$ and $\mathbf{I}_i$ is the identity matrix of order i.

The displacement field for all kinds of strip elements can be obtained by interpolation in terms of the nodal line displacements in y-direction:

$$\mathbf{u}_j = \begin{Bmatrix} u_{0j} \\ \psi_{xj} \\ v_{0j} \\ \psi_{yj} \\ w_{0j} \end{Bmatrix} = \mathbf{N}(y)\mathbf{W}_j(x) = \begin{bmatrix} \mathbf{N}_1(y) \\ \mathbf{N}_2(y) \\ \mathbf{N}_3(y) \\ \mathbf{N}_4(y) \\ \mathbf{N}_5(y) \end{bmatrix} \mathbf{W}_j(x), \tag{6}$$

where $\mathbf{N}(y)$ is the shape function matrix for the nodal line displacement interpolation and j is the serial number of the strip element.

Therefore, the relationship between the strain and the nodal line displacement vector for the j-th strip element is

$$\boldsymbol{\varepsilon}_j = [\mathbf{B}_0 \quad \mathbf{B}_1] \begin{Bmatrix} \mathbf{W}_j \\ \mathbf{W}_{j,x} \end{Bmatrix}, \tag{7}$$

where transverse normal strains are ignored and

$$\boldsymbol{\varepsilon}_j = \{\varepsilon_{1j} \quad \varepsilon_{2j} \quad \varepsilon_{4j} \quad \varepsilon_{5j} \quad \varepsilon_{6j}\}^T,$$

$$\mathbf{B}_0 = [\mathbf{0}_{15\times 1} \quad \left(\mathbf{N}_{3,y} + z\mathbf{N}_{4,y}\right)^T \ \left(\mathbf{N}_{5,y} + \mathbf{N}_4\right)^T \quad (\mathbf{N}_2)^T \quad \left(\mathbf{N}_{1,y} + z\mathbf{N}_{2,y}\right)^T]^T,$$

$$\mathbf{B}_1 = [(\mathbf{N}_1 + z\mathbf{N}_2)^T \quad \mathbf{0}_{15\times 1} \quad \mathbf{0}_{15\times 1}\ (\mathbf{N}_5)^T \quad (\mathbf{N}_3 + z\mathbf{N}_4)^T]^T.$$

For an orthotropic layer, the constitutive relations are given in the form

$$\boldsymbol{\sigma}_j = \bar{\mathbf{Q}}_j\boldsymbol{\varepsilon}_j, \tag{8}$$

where $\bar{\mathbf{Q}}_j$ is the stiffness matrix of the layer, and

$$\boldsymbol{\sigma}_j = \{\sigma_{1j} \quad \sigma_{2j} \quad \sigma_{4j} \quad \sigma_{5j} \quad \sigma_{6j}\}^T.$$

The potential energy for the j-th strip element is written as

$$L_j = \frac{1}{2}\int_x \int_y \left[\int_z \boldsymbol{\sigma}_j^T \boldsymbol{\varepsilon}_j dz + N_{xj}\left(\frac{\partial w_j}{\partial x}\right)^2 + N_{yj}\left(\frac{\partial w_j}{\partial y}\right)^2 + 2N_{xyj}\frac{\partial w_j}{\partial x}\frac{\partial w_j}{\partial y}\right] dydx, \tag{9}$$

where N_{xj}, N_{yj} and N_{xyj} are membrane forces in the j-th strip element.

Substituting Eqs. (7) and (8) into Eq. (9), we have

$$L_j = \frac{1}{2}\int_{-a/2}^{a/2} \left(\mathbf{W}_{j,x}^T\mathbf{k}_{11j}\mathbf{W}_{j,x} + 2\mathbf{W}_j^T\mathbf{k}_{01j}\mathbf{W}_{j,x} + \mathbf{W}_j^T\mathbf{k}_{00j}\mathbf{W}_j\right) dx, \tag{10}$$

in which $\mathbf{k}_{11j}$, $\mathbf{k}_{01j}$, $\mathbf{k}_{00j}$ are called the strip stiffness matrices whose detailed expressions are not listed here.

Multiplying the potential energies of all strip elements and then applying the variational principle, we have

$$\frac{1}{2}\sum_{j=1}^{NS}\delta\int_{-a/2}^{a/2}\left(\mathbf{W}_{j,x}^{T}\mathbf{k}_{11j}\mathbf{W}_{j,x}+2\mathbf{W}_{j}^{T}\mathbf{k}_{01j}\mathbf{W}_{j,x}+\mathbf{W}_{j}^{T}\mathbf{k}_{00j}\mathbf{W}_{j}\right)dx=0. \tag{11}$$

Now introducing the global nodal line displacement vector $\mathbf{\Phi}(x)=\left\{\mathbf{u}_1^T \quad \boldsymbol{\lambda}_1^T \quad \mathbf{u}_2^T\cdots\boldsymbol{\lambda}_{NS}^T \quad \mathbf{u}_{NS+1}^T\right\}^T$, Eq. (11) can be reduced to

$$\frac{1}{2}\delta\int_{-a/2}^{a/2}\left(\mathbf{\Phi}_{,x}^{T}\mathbf{K}_{11}\mathbf{\Phi}_{,x}+2\mathbf{\Phi}^{T}\mathbf{K}_{01}'\mathbf{\Phi}_{,x}+\mathbf{\Phi}^{T}\mathbf{K}_{00}\mathbf{\Phi}\right)dx=0, \tag{12}$$

where $\mathbf{K}_{11}$, $\mathbf{K}_{01}'$ and $\mathbf{K}_{00}$ are global stiffness matrices. For the general super-unit, they are assembled with $\mathbf{k}_{11j}$, $\mathbf{k}_{01j}$ and $\mathbf{k}_{00j}$ in the same way as in finite element analysis. But for the delaminated super-unit, the stiffness matrices of the delamination tip strip element k become $\bar{\mathbf{T}}_{km}^{T}\mathbf{k}_{11k}\bar{\mathbf{T}}_{km}$, $\bar{\mathbf{T}}_{km}^{T}\mathbf{k}_{01k}\bar{\mathbf{T}}_{km}$ and $\bar{\mathbf{T}}_{km}^{T}\mathbf{k}_{00k}\bar{\mathbf{T}}_{km}$ in the assembling process.

Setting the variation of Eq. (12) with respect to Φ, we can obtain

$$\delta\mathbf{\Phi}^{T}\left(\mathbf{K}_{11}\mathbf{\Phi}_{,xx}-\mathbf{K}_{01}\mathbf{\Phi}_{,x}-\mathbf{K}_{00}\mathbf{\Phi}\right)=0, \tag{13}$$

$$\delta\mathbf{\Phi}^{T}\left(\mathbf{K}_{11}\mathbf{\Phi}_{,x}+\mathbf{K}_{01}'^{\mathrm{T}}\mathbf{\Phi}\right)|_{x=\pm a/2}=0, \tag{14}$$

with $\mathbf{K}_{01}=\mathbf{K}_{01}'-\mathbf{K}_{01}'^{T}$.

If all components in $\delta\mathbf{\Phi}$ are independent, the force equilibrium equations and the boundary conditions can be deduced from Eqs. (13) and (14) directly. But if there are known or specified displacements in $\mathbf{\Phi}$, $\delta\mathbf{\Phi}$ is dependent and those dependent components in the vector $\delta\mathbf{\Phi}$ must be eliminated. Supposing that there are N_1 unknown displacement components denoted by the vector $\boldsymbol{\varphi}\in R^{N_1}$ and N_2 known displacement components denoted by the vector $\bar{\boldsymbol{\varphi}}\in R^{N_2}$, respectively, $\mathbf{\Phi}$ can be decomposed into

$$\mathbf{\Phi}=\mathbf{T}_1\boldsymbol{\varphi}+\mathbf{T}_2\bar{\boldsymbol{\varphi}}, \tag{15}$$

where $\mathbf{T}_j\in R^{(N_1+N_2)\times N_j}$ $(j=1,2)$ is the row transfer matrix and $\delta\varphi=0$. Substituting Eq. (15) into Eqs. (13) and (14), we can get the force equilibrium equations and the boundary conditions as follows:

$$\bar{\mathbf{K}}_{11}\boldsymbol{\varphi}_{,xx}-\bar{\mathbf{K}}_{01}\boldsymbol{\varphi}_{,x}-\bar{K}_{00}\boldsymbol{\varphi}=\bar{\mathbf{Q}}_{\varphi}, \tag{16}$$

$$\delta\boldsymbol{\varphi}^{\mathrm{T}}\left(\mathbf{\Pi}\boldsymbol{\varphi}-\mathbf{S}_{\varphi}\right)|_{x=\pm a/2}=0, \tag{17}$$

in which

$$\bar{\mathbf{K}}_{11}=\mathbf{T}_1^{T}\mathbf{K}_{11}\mathbf{T}_1,\quad \bar{\mathbf{K}}_{01}=\mathbf{T}_1^{T}\mathbf{K}_{01}\mathbf{T}_1,\quad \bar{\mathbf{K}}_{00}=\mathbf{T}_1^{T}\mathbf{K}_{00}\mathbf{T}_1,$$

$$\bar{\mathbf{Q}}_{\varphi}=\mathbf{T}_1^{T}\left(\mathbf{K}_{01}\frac{\partial}{\partial x}+\mathbf{K}_{00}-\mathbf{K}_{11}\frac{\partial^2}{\partial x^2}\right)\mathbf{T}_2\bar{\boldsymbol{\varphi}},$$

$$\mathbf{\Pi}=\mathbf{T}_1^{T}\mathbf{K}_{01}'^{T}\mathbf{T}_1+\mathbf{T}_1^{T}\mathbf{K}_{11}\mathbf{T}_1\frac{\partial}{\partial x},$$

$$\mathbf{S}_{\varphi}=-\mathbf{T}_1^{T}\mathbf{K}_{01}'^{T}\mathbf{T}_2\bar{\boldsymbol{\varphi}}-\mathbf{T}_1^{T}\mathbf{K}_{11}\mathbf{T}_2\bar{\boldsymbol{\varphi}}_{,x}.$$

3 The distributed transfer function solution to the super-unit

Defining the state variable vector

$$\boldsymbol{\eta}(x) = \left\{ \boldsymbol{\varphi}^T(x) \ \frac{\partial}{\partial x}\boldsymbol{\varphi}^T(x) \right\}^T \in R^{2N_1}, \tag{18}$$

Eqs. (16) and (17) can be written in an equivalent state equation form as

$$\boldsymbol{\eta}_{,x} = \mathbf{F}\boldsymbol{\eta}(x) + \mathbf{f}, \quad x \in (-a/2,\ a/2), \tag{19.1}$$

$$\mathbf{M}_b\boldsymbol{\eta}(-a/2) + \mathbf{N}_b\boldsymbol{\eta}(a/2) = \boldsymbol{\gamma}_b, \tag{19.2}$$

where $\mathbf{F}$, $\mathbf{M}_b$ and $\mathbf{N}_b$, and $\boldsymbol{\gamma}_b$ are called state-space matrix, boundary matrix, and boundary disturb vector of the super-unit, respectively.

Following [9], the solution to Eq. (19) is obtained as

$$\boldsymbol{\eta}(x) = \mathbf{H}(x)\boldsymbol{\gamma}_b + \int_{-a/2}^{a/2} \mathbf{G}(x,\xi)\mathbf{f}(\xi)d\xi \tag{20}$$

with

$$\mathbf{G}(x,\xi) = \begin{cases} \mathbf{H}(x)\mathbf{M}_b e^{-\mathbf{F}(a/2+\xi)} & \xi \le x, \\ -\mathbf{H}(x)\mathbf{N}_b e^{\mathbf{F}(a/2-\xi)} & \xi > x, \end{cases}$$

$$\mathbf{H}(x) = e^{\mathbf{F}x}\left[\mathbf{M}_b e^{-\mathbf{F}a/2} + \mathbf{N}_b e^{\mathbf{F}a/2}\right]^{-1}.$$

4 The buckling analysis for laminates with built-in delamination

A rectangular plate with a bulit-in delamination shown in Fig. 4 can be divided into three super-units $\Omega_1(AEHD)$, $\Omega_2(EFGH)$ and $\Omega_3(FBCG)$. $\Omega_2(EFGH)$ is the one including a delamination. For every rectangular super-unit, there are two types of nodes: the boundary nodes

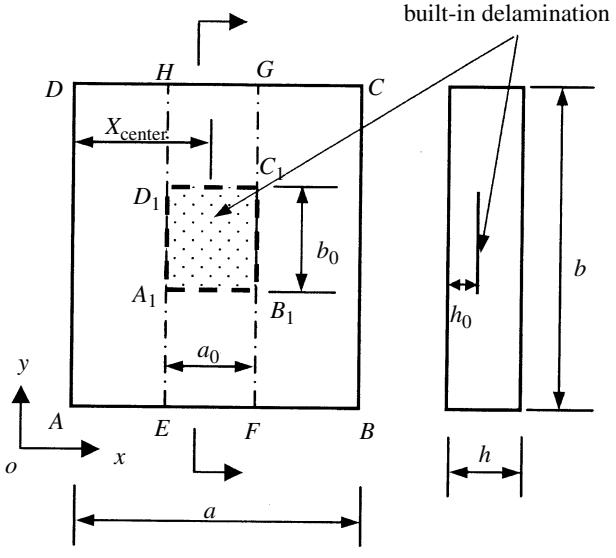

Fig. 4. The plate with a built-in delamination

where boundary conditions are prescribed, and the inter-connecting nodes where the neighboring super-units are inter-connecting.

For the general super-unit without delaminations, the length of the strip element is assumed as a_i, and then the nodal line displacements are defined in the domain $-a_i/2 \le x \le a_i/2$. Assume that there are N_c^i unknown displacements at the inter-connecting nodes that are denoted by the vector $\boldsymbol{\varphi}_c^i$, and N_b^i boundary conditions at boundary nodes that are represented by the vector $\boldsymbol{\gamma}_b^i (i = 1, 3)$. The state space vector of the super-unit can be decomposed into the following form:

$$\boldsymbol{\eta}^i(x) = \boldsymbol{\eta}_{eb}^i(x) + \mathbf{H}_{\varphi}^i(x)\boldsymbol{\varphi}_c^i \tag{21}$$

with

$$\boldsymbol{\eta}_{eb}^i(x) = \int_{-a_i/2}^{a_i/2} \mathbf{G}^i(x,\xi)\mathbf{f}(\xi)d\xi + \mathbf{H}_b^i(x)\boldsymbol{\gamma}_b^i \left[\mathbf{H}_b^i(x)\ \mathbf{H}_{\varphi}^i(x)\right] = \mathbf{H}^i(x).$$

For the delaminated super-unit Ω_2, it should be noted that there are two unknown inter-connecting nodes n_1 and n_2 in Ω_2 connecting to another inter-connecting node n in Ω_1 or Ω_3 at the delamination tip (A_1D_1 or B_1C_1 in Fig. 4) as shown in Fig. 5. The relationship between the node displacements $\mathbf{u}_n^k$ (corresponding to node n_k, $k = 1, 2$) and $\mathbf{u}_n$ (corresponding to node n) is analogous to that between $\mathbf{u}_m^k(x)$ and $\mathbf{u}_m(x)$ in Eq. (4) and can be expressed as

$$\mathbf{u}_n^k = \mathbf{T}_{nk}\mathbf{u}_n. \tag{22}$$

Therefore, the unknown inter-connecting node displacements of the delaminated super-unit could be expressed by those of the general super-unit Ω_1 or Ω_3

$$\boldsymbol{\varphi}_c^2 = \bar{\mathbf{T}}_{nk}\boldsymbol{\varphi}_c, \tag{23}$$

where $\boldsymbol{\varphi}_c = \left[\left(\boldsymbol{\varphi}_c^1\right)^T \quad \left(\boldsymbol{\varphi}_c^3\right)^T\right]^T$, and $\bar{\mathbf{T}}_{nk}$ is constructed with $\mathbf{T}_{nk}$. Then the state space vector of the super-unit Ω_2 can be expressed in the following form:

$$\boldsymbol{\eta}^2(x) = \boldsymbol{\eta}_{eb}^2(x) + \mathbf{H}_{\varphi}^2(x)\bar{\mathbf{T}}_{nk}\boldsymbol{\varphi}_c. \tag{24}$$

So, the responses of all super-units are expressed in terms of $\boldsymbol{\varphi}_c$. Consequently, displacement continuity conditions at the inter-connecting nodes are satisfied automatically.

Let $\mathbf{S}_c^i (i = 1, 2, 3)$ be the internal force vector applied at the inter-connecting node in the rectangular super-unit i and $x_c = -a_i/2$ or $a_i/2$ the position of the inter-connecting node in x-direction. We then have

$$\mathbf{S}_c^i = \boldsymbol{\Pi}_c^i\boldsymbol{\eta}(x_c), \tag{25}$$

in which the matrix $\boldsymbol{\Pi}_c^i$ is derived from $\boldsymbol{\Pi}_j$ in Eq. (18) and represents the relationship between the internal forces and displacements.

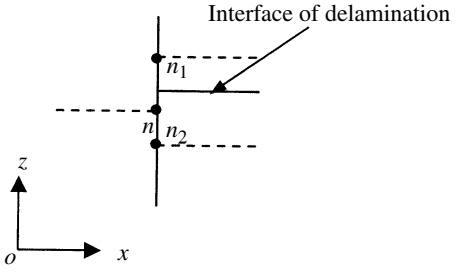

Fig. 5. Relation among displacements of the node at the delamination tip

For the general super-unit, according to Eqs. (21) and (25), we have

$$\mathbf{S}_c^i = -\mathbf{K}_c^i \boldsymbol{\varphi}_c^i + \mathbf{q}_c^i, \tag{26}$$

where $\mathbf{K}_c^i = -\mathbf{\Pi}_c^i \mathbf{H}_\varphi^i(x)$ is the stiffness matrix of the super-unit. $\mathbf{q}_c^i = \mathbf{\Pi}_c^i \boldsymbol{\eta}_{eb}^i(x)$ represents the inner transfer force generated by the action of external loads and the boundary disturbing force at the inter-connecting node.

For the delaminated super-unit, there are two inter-connecting nodes n_1 and n_2 connecting to another inter-connecting node n in the general super-unit at the delamination tip as shown in Fig. 5. Therefore, the internal force at node n is equal to the sum of those at nodes n_1 and n_2 referring to node n. According to Eqs. (24) and (25), we have

$$\mathbf{S}_c^2 = -\mathbf{K}_c^2 \boldsymbol{\varphi}_c + \mathbf{q}_c^2, \tag{27}$$

where

$$\mathbf{K}_c^2 = \begin{bmatrix} \mathbf{K}_c^{21} \bar{\mathbf{T}}_{nk} \\ \bar{\bar{\mathbf{T}}}_{n1} \mathbf{K}_{c1}^{22} \bar{\mathbf{T}}_{nk} + \bar{\bar{\mathbf{T}}}_{n2} \mathbf{K}_{c2}^{22} \bar{\mathbf{T}}_{nk} \end{bmatrix},$$

$$\mathbf{\Pi}_c^2 \mathbf{H}_\varphi^2(x) = -\left[\left(\mathbf{K}_c^{21}\right)^T \quad \left(\mathbf{K}_{c1}^{22}\right)^T \quad \left(\mathbf{K}_{c2}^{22}\right)^T \right]^T,$$

and $\bar{\bar{\mathbf{T}}}_{n1}$ and $\bar{\bar{\mathbf{T}}}_{n2}$ are internal force transfer matrices corresponding to the top and bottom sublaminates and composed of $(\mathbf{T}_{n1})^T$ and $(\mathbf{T}_{n2})^T$, respectively. $\mathbf{K}_c^{21}$, $\mathbf{K}_{c1}^{22}$ and $\mathbf{K}_{c2}^{22}$, which construct the stiffness matrix of the super-unit, are composed of corresponding rows of $\mathbf{\Pi}_j$ in Eq. (17) at nodes n, n_1 and n_2, respectively. The meaning of $\mathbf{q}_c^2 = \mathbf{\Pi}_c^2 \boldsymbol{\eta}_{eb}^2(x)$ is the same as of $\mathbf{q}_c^i$ in Eq. (26).

If we assume that the internal force $\mathbf{S}_c^i$ and the external force $\mathbf{q}_e$ are exerted at the connecting node, and let the general displacement vector be $\boldsymbol{\varphi}_c$, according to force balance of nodes $\mathbf{S}_c^i + \mathbf{q}_e = \mathbf{0}$, we can get the equilibrium equations at those connecting nodes in the following form:

$$\mathbf{K}_c \boldsymbol{\varphi}_c = \mathbf{q}_c + \mathbf{q}_e, \tag{28}$$

where the general stiffness matrix $\mathbf{K}_c$ and the node force vector $\mathbf{q}_c$ are assembled with $\mathbf{K}_c^i$ and $\mathbf{q}_c^i$, and the assembling method is similar to that of the finite element method.

For the buckling problems of the axial-compression delaminated rectangular plates, there is $\mathbf{q}_c = \mathbf{q}_e = \mathbf{0}$. Then the equilibrium equations at those connecting nodes turn into the buckling equations

$$\mathbf{K}_c \boldsymbol{\varphi}_c = \mathbf{0}. \tag{29}$$

At the buckling point $\boldsymbol{\varphi}_c \neq \mathbf{0}$, so the characteristic equation for the delaminated plate is

$$|\mathbf{K}_c| = 0. \tag{30}$$

Solving Eq. (30), we can get the critical buckling load. Then the corresponding buckling mode can be deduced from Eqs. (29), (21) and (24).

5 Numerical examples analysis

Here, the shape function matrix is first introduced for the strip displacement interpolation.

The displacement vector at the nodal line is given in Eq. (2). The displacement vector $\boldsymbol{\lambda}_j(x)$ at the inner nodal line is defined as

$$\boldsymbol{\lambda}_j(x) = \left\{ u_{0j}\left(x, \frac{b_j}{2}\right) \psi_{xj}\left(x, \frac{b_j}{2}\right) v_{0j}\left(x, \frac{b_j}{2}\right) \psi_{yj}\left(x, \frac{b_j}{2}\right) w_{0j}\left(x, \frac{b_j}{2}\right) \right\}^T, \tag{31}$$

and the corresponding shape function matrix is given as

$$\mathbf{N}(y) = \begin{bmatrix} (1 - 3\xi + 2\xi^2) \cdot \mathbf{I}_5 \\ (4\xi - 4\xi^2) \cdot \mathbf{I}_5 \\ -(\xi - 2\xi^2) \cdot \mathbf{I}_5 \end{bmatrix}^T, \tag{32}$$

where $\zeta = y/b_j, b_j$ is the width of the j-th strip element.

In all numerical examples, assume that the delaminated plate is compressed only in the x-direction. The delaminated region is divided into two parts (Fig. 4): the thinner sublaminate (sublaminate 1) and the thicker one (sublaminate 2). If there are no additional explanations, the delaminated plate of $a/b = 1$ and $h/a = 5$ is clamped at two ends in the x-direction and free at two ends in the y-direction. The parameters $\alpha = a_0/a$, $\gamma = b_0/b$ and $\beta = h_0/h$ are rates of the delamination to plate in length, width and thickness direction, respectively. $\bar{P}_{cr} = \frac{3P_{cr}a^2(1-v_{12}v_{21})}{\pi^2 E_1 h^3}$ is the dimensionless buckling load of the delaminated plate. Here, P_{cr} is the buckling load of the delaminated plate E_1, v_{12} and v_{21} are engineering constants of the layer and replaced by $E_1 = E$ and $v_{12} = v_{21} = v$ for the isotropic layer.

5.1 Buckling load of the plate with through-the-width delamination

Firstly, for the isotropic plate of $a/h = 4$, $a/b = 4$ and $\beta = 0.4$, Fig. 6 gives a comparison of the results in this paper to those from the first (FSDT) and the third (HSDT) order deformation theory analytic solutions of a beam (Li and Zhou [8]) and the finite element software NASTRAN. The material parameters are $E = 215$ GPa and $v = 0.26$. We can see from Fig. 6 that for the same delamination the buckling load of the four methods differs little. Global, mixed and local buckling modes all appear and the changing trends of the four types are identical. All this indicates that our method is correct. Additionally, we can also see that the

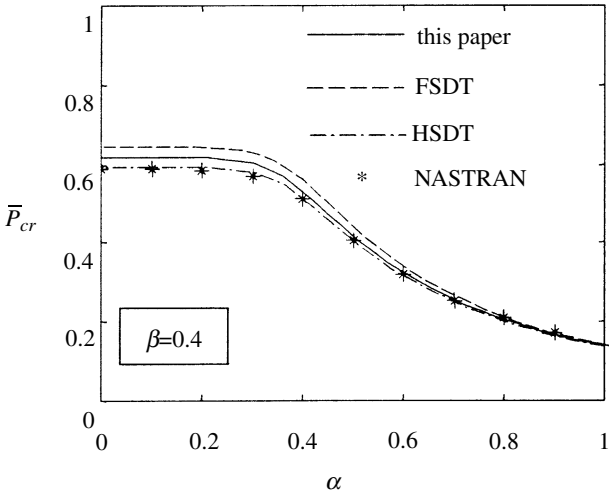

Fig. 6. Buckling load of the plate with through-the-width delamination

theory of the plate is more rational than that of the beam for the one-dimensional delamination problem.

5.2 Effects of depth, size and position of built-in rectangular delamination

For a symmetric delaminated plate of varied delamination length and $\gamma = 0.5$, the relationship between buckling load and depth of the delamination is given in Fig. 7. It can be seen that, as the depth of the delamination ($0 < \beta \leq 0.5$) increases, the buckling load tends to increase and the buckling mode of the delaminated plate changes from local mode to mixed mode and then to global mode generally. But for the delaminated plates of $\alpha = 0.9$, the global mode doesn't appear and the buckling load decreases slightly as the depth of the delamination increases when $\beta > 0.35$ The reason is that the stiffness of the sublaminate 2 decreases as the depth of the delamination increases and α is bigger than γ, and the buckling load decreases in the mixed buckling process.

Figure 8 gives the relationship between the buckling load and the length (Fig. 8a, $\gamma = 0.5$) or the width (Fig. 8b $\alpha = 0.5$) of the delamination for the symmetric delaminated plate. From the two figures, it can be seen that the buckling load decreases as the size of the delamination increases. In this case, the buckling mode transforms from global to local mode via mixed mode.

For the delaminated plate of $\beta = 0.4$, Fig. 9 gives the variation of the buckling load as the position of the delamination varies in x-direction. By comparing those curves, we can see that for different sizes of the delamination the relationship between the buckling load and the position of the delamination is different because the buckling mode is different. When $\alpha = \gamma \leq 0.3$, a global buckling mode appears, the buckling load of the delaminated plate decreases first and then increases as the delamination closes to the center of the plate. The effect of the delamination on the plate is smallest when the delamination lies at the center of the plate. When $\alpha = \gamma = 0.4 \sim 0.6$, a mixed buckling mode appears, the buckling load of the delaminated plate increases as the delamination closes to the center of the plate. When $\alpha = \gamma \leq 0.7 \sim 0.8$, a local buckling mode appears, the buckling load of the delaminated plate decreases as the delamination closes to the center of the plate.

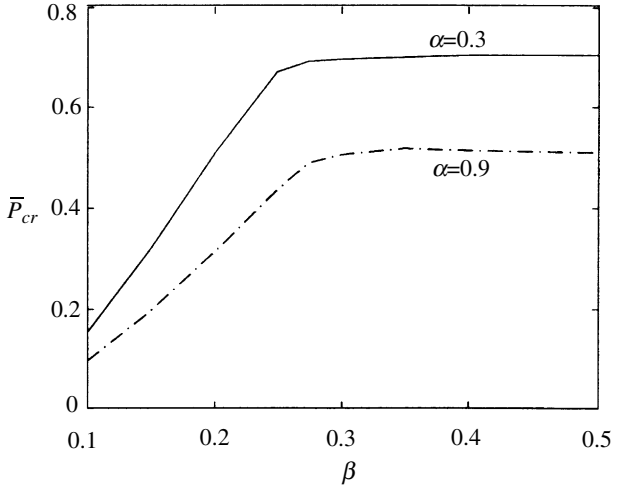

Fig. 7. Effect of the depth of the delamination on the buckling load

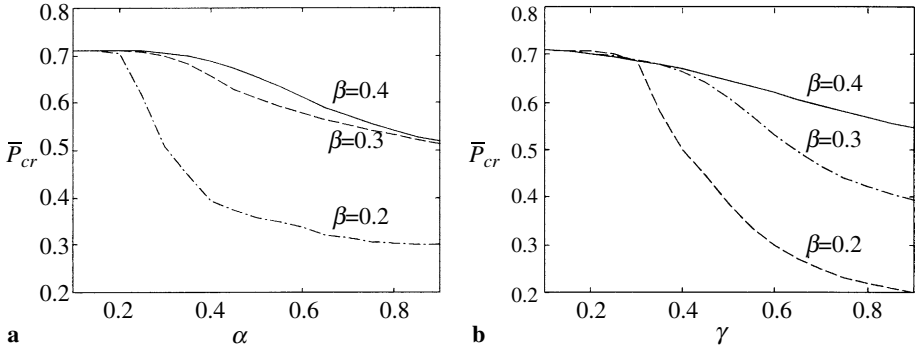

Fig. 8. Effect of the size of the delamination on the buckling load: **a** size of delamination varying on the x-coordinate, **b** size of delamination varying on the y-coordinate

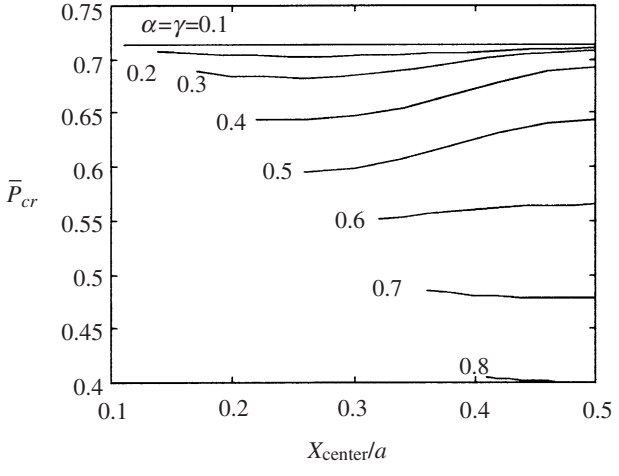

Fig. 9. Effect of the position of delamination on the buckling load

5.3 Effects of plying angle and boundary conditions

For the delaminated laminates, the buckling load and mode vary with the plying angle (Fig. 10). The composite material used in Fig. 10 is Kevlar-epoxy whose material constants are: $E_1 = 144.8$ GPa, $E_2 = 9.65$ GPa, $G_{12} = G_{13} = 4.14$ GPa, $G_{23} = 3.45$ GPa, $v_{12} = 0.3$. The plying sequence of the laminate is $[\theta/(90^\circ - \theta)/\theta]_{10}$ and two ends of the laminate in x-direction are clamped. The delamination $\alpha = \gamma = 0.5$ is symmetric in-plane. From Fig. 10, we see that the buckling load of the delaminated laminate decreases first and then increases, but for the different depth delamination, θ corresponding to the minimum point is different. When $\beta = 0.4$ or $\beta = 0.2$, the buckling mode of the delaminated laminate is global or mixed, θ corresponding to the minimum point is around 45°. When $\beta = 0.1$, the buckling mode of the delaminated laminate is local, θ corresponding to the minimum value of $\overline{P}_{cr}$ being around 75°.

From Fig. 10, we can also find the effect of the boundary condition on the buckling load. When $\beta = 0.4$, the buckling load of the laminate with two clamped ends in y-direction (called "clamped laminate" in the following) is higher than that of the laminate with two free ends in y-direction (called "free laminate" in the following), although the buckling modes of the two

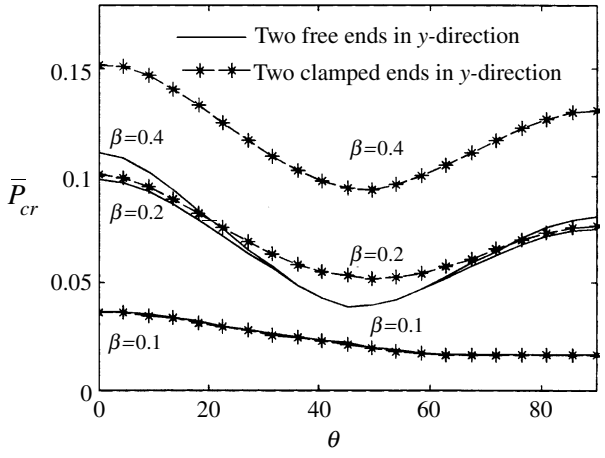

Fig. 10. Effect of the plying angle of the laminate on the buckling load

types of laminate are both global modes. When $\beta = 0.2$, the mixed mode appears in the clamped laminate. The buckling mode of the free laminate is global around $\theta = 45^\circ$ and the buckling load is almost the same as that of the free laminate of $\beta = 0.4$. But when θ is far away from 45°, a mixed mode appears in it and its buckling load is close to that of the clamped laminate of $\beta = 0.2$. When $\beta = 0.1$, since the local mode appears in both types, the effect of the boundary condition is smaller as well as the difference between the buckling loads of the two types.

6 Conclusions

The buckling problem of the composite laminate with a built-in delamination is analyzed using the strip transfer function method. Results indicate that the effects of length, depth and position of the delamination, together with the boundary conditions and the plying angle of the material, on the buckling load and mode of the plate with built-in delamination are obvious. There are three buckling modes (the local mode, the mixed mode and the global mode) for the delaminated plate. For different buckling modes, the effect of each factor on the buckling load is different. The analysis in this paper offers some basic results for researching the buckling problem of the plate with built-in delamination.

Acknowledgements

This project is sponsored by grants from the National Outstanding Youth Found of the P. R. China (No. 19925209) and the Provincial Natural Science Found of Hu-Nan, P. R. China (No. 02JJY2009).

References

[1] Chen, S., Li, S.: A study of two-dimensional delamination buckling in a symmetrical laminate. J. Shanghai Jiaotong Univ. **7**, 89–98 (1990) (in Chinese).

[2] Li, S. Chen, S.: An experimental study of delamination buckling failure in a laminate with a single elliptic, or rectangular or triangular disbond. Acta Mater. Compos. Sinica **7**, 89–98 (1990) (in Chinese).

[3] Yin, W. L., Jane, K. C.: Refined buckling and postbuckling analysis of two-dimensional delamination-I. Analysis and validation. Int. J. Solids Struct. **29**, 591–610 (1992).
[4] Yin, W. L., Jane, K. C.: Refined buckling and postbuckling analysis of two-dimensional delamination-II. Results for anisotropic laminates and conclusion. Int. J. Solids Struct. **29**, 611–639 (1992).
[5] Zhang, X., Yu, S.: The growth simulation of circular buckling-driven delamination. Int. J. Solids Struct. **36**, 1799–1821 (1999).
[6] Whitcomb, J. D.: Three-dimensional analysis of a postbuckled embedded delamination. J. Comp. Mater. **23**, 862–889 (1989).
[7] Sun, X., Chen, H., Su, C. Liu, X.: Delamination growth in composite laminates. Acta Mech. Sinica **32**, 224–231 (2000) (in Chinese).
[8] Li, D., Zhou, J.: Buckling analysis of delaminated beam for the high-order shear deformation theory. Acta Mech. Sol. Sinica **21**, 225–233 (2000) (in Chinese).
[9] Zhou, J. Yang, B.: Strip distributed transfer function method for analysis of plates. Int. J. Num. Meth. Engng. **39**, 1915–1932 (1996).

Authors' address: D. Li, G. Tang and J. Zhou, College of Aerospace and Material Engineering, National University of Defense Technology, Changsha, Hu-Nan Province, 410073, P.R. China (E-mail: daokuili@yahoo.com.cn)